IOPscience iopscience.iop.org

Home Search Collections Journals About Contact us My IOPscience

Resistance Switching in $Ni/HfO_x/Ni$ Nonvolatile Memory Device with CF_4/O_2 Plasma Post-treatment

This content has been downloaded from IOPscience. Please scroll down to see the full text.

2012 Jpn. J. Appl. Phys. 51 01AJ10

(http://iopscience.iop.org/1347-4065/51/1S/01AJ10)

View the table of contents for this issue, or go to the journal homepage for more

Download details:

IP Address: 140.113.38.11

This content was downloaded on 28/04/2014 at 22:35

Please note that terms and conditions apply.

DOI: 10.1143/JJAP.51.01AJ10

Resistance Switching in Ni/HfO$_x$/Ni Nonvolatile Memory Device with CF$_4$/O$_2$ Plasma Post-treatment

Chiung-Hui Lai*, Te-Shun Chang, Wen-Hsien Tzeng[1], and Kow-Ming Chang[1,2]

Department of Electronics Engineering, Chung Hua University, Hsinchu 300, Taiwan, R.O.C.
[1] *Institute of Electronics, National Chiao Tung University, Hsinchu 300, Taiwan, R.O.C.*
[2] *Department of Electronic Engineering, I Shou University, Kaohsiung 840, Taiwan, R.O.C.*

Received May 12, 2011; accepted August 25, 2011; published online January 20, 2012

The resistance switching characteristics of Ni/HfO$_x$/Ni capacitor structures with CF$_4$/O$_2$ plasma post-treatment of different gas flow rate ratios were investigated. The HfO$_x$ film was deposited by an electron-gun evaporator, followed by the CF$_4$/O$_2$ plasma post-treatment with different gas flow rate ratios. According to the filament model, conducting filaments (CFs) are formed by the percolation of various types of defects such as oxygen ions and oxygen vacancies. Moreover, the incorporation of oxygen/fluorine may terminate the oxygen vacancies to form Hf–F bonds and eliminate both fixed and interface traps, which can help to form fixed CFs in the film owing to local stronger Hf–F bonds. In this work, the improvement in the stability of resistance switching and current in the high-resistance state (HRS) was achieved by suitable plasma post-treatment. This may be attributed to the formation of Hf–F bonds as observed through electron spectroscopy for chemical analysis.
© 2012 The Japan Society of Applied Physics

1. Introduction

Resistance random access memory (RRAM) has attracted much attention owing to its possible application to high-density and low-cost nonvolatile memory devices with high performance.[1–3] Transition-metal oxide (TMO)-based RRAM devices exhibit excellent characteristics such as low power, high speed, good scalability, and high-density integration.[4,5] TMO materials, such as NiO, TiO_2, Al_2O_3, and HfO_2, show very promising potential for RRAM because of their simple composition, low production cost, and compatibility with complementary-metal–oxide–semiconductor (CMOS) technology.[6–11] Recently, the electrical characteristics of HfO_2-based RRAM devices have been reported.[12–14] One of the proposed models for resistance switching is the formation of conducting filaments (CFs) or paths by applying a sufficiently high voltage. However, owing to the high energy band gap, HfO_2-based RRAM with high resistance has suffered from the nonuniformity of operation parameters, poor endurance, and low device yield.[15] It has been reported that fluorine (F) incorporation can reduce the fixed charge and passivate interface traps, resulting from the segregation of F in the HfO_2/SiO_2 interfaces and the passivation of oxygen vacancies and interface traps by the formation of stronger Hf–F bonds.[16–20] Furthermore, the formation of HfO_2 films by electron gun (e-gun) evaporation at low temperatures is very cost-effective.

In this work, to obtain satisfactory HfO_2 film quality for its use as an insulator in RRAM with a bipolar resistance switching (BRS) operation mode, we demonstrate the effect of different proportions of F incorporated in the HfO$_x$ film on the stability of resistance switching of a Ni/HfO$_x$/Ni RRAM.

2. Experiment

A schematic diagram of the resistive memory devices in this study is illustrated in Fig. 1. A thermally oxidized (500 nm SiO_2) p-type silicon wafer was used as a substrate, onto which 50-nm-thick nickel (Ni) metal was deposited as a bottom electrode by e-gun evaporation at 25 °C. Then, a HfO$_x$ film with a thickness of 30 nm was directly deposited on the Ni/SiO_2/Si substrate by the e-gun evaporation system using a pure HfO_2 target. The chamber pressure and substrate temperature were maintained at 2×10^{-6} Torr and 25 °C, respectively. Afterwards, CF$_4$/O$_2$ plasma post-treatment was performed on the HfO_2 surface with an inductively coupled plasma (ICP) power of 500 W and a process pressure of 0.1 Torr in a high-density-plasma chemical vapor deposition (HDP-CVD) system at 150 °C for 90 s. The flow rate ratio of the CF$_4$/O$_2$ gas mixture was 50/5 or 10/40 sccm. After the plasma post-treatment, a 50-nm-thick Ni top electrode was deposited on the HfO_2 films by e-gun evaporation at 25 °C to complete the metal/insulator/metal (MIM) memory cell. For comparison, a reference sample made without CF$_4$/O$_2$ plasma post-treatment was also prepared by the same process.

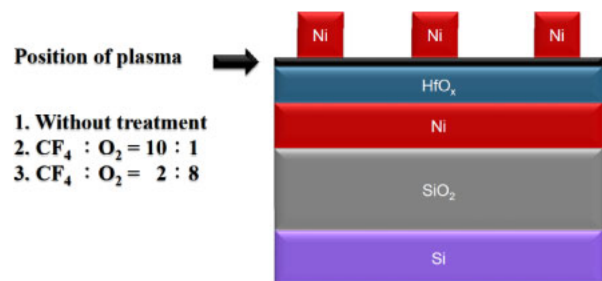

Fig. 1. (Color online) Schematic diagram of resistive memory devices with different CF$_4$/O$_2$ plasma post-treatment conditions.

The crystal structure, concentration depth profile, and chemical bonds were analyzed by X-ray diffraction (XRD) patterns, Auger electron spectrometry (AES), and electron spectroscopy for chemical analysis (ESCA), respectively. The current–voltage (I–V) characteristics of the devices were studied using an Agilent 4156 A semiconductor parameter analyzer.

3. Results and Discussion

Figure 2(a) shows the typical I–V characteristics of the RRAM with the Ni/HfO$_x$/Ni capacitor structure without CF$_4$/O$_2$ plasma post-treatment. The bias was applied to the top electrode while the bottom electrode was grounded during the dc voltage sweep measurements at room temperature.

*E-mail address: chlai@chu.edu.tw

 © 2012 The Japan Society of Applied Physics

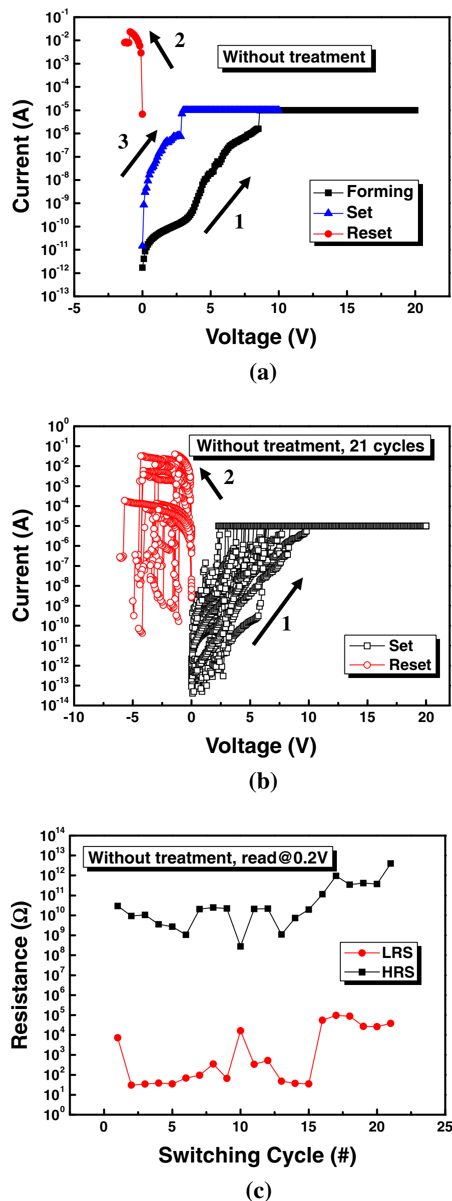

Fig. 2. (Color online) (a) Typical current–voltage (I–V) characteristics of RRAM with Ni/HfO_2/Ni capacitor structure, (b) I–V curves for 21 cycles of voltage sweeping, (c) endurance properties for the device without plasma treatment.

BRS between the high-resistance state (HRS) and low-resistance state (LRS) was induced by the applied voltage. A forming process with a compliance current was required to activate the as-deposited cell while preventing electrical breakdown. The forming voltage of the device was approximately 8 V with a compliance current of 10 μA. After the forming process, the device entered the LRS. By sweeping a negative bias above the reset voltage (V_{reset}) of approximately -1.3 V, an abrupt decrease in current was observed, where the cell switches from the LRS to HRS, called the reset process. Conversely, the cell returned to the LRS upon applying a positive bias above the set voltage (V_{set}) of approximately 1.1 V, called the set process. Figure 2(b) shows I–V curves for 21 cycles of voltage sweeping for the device without plasma treatment. Unfortunately, this device exhibited an unstable reset voltage and a different resistance in each process. A higher process current was observed at a low positive voltage in the HRS. These results may be due to defects in the HfO_x film, such as oxygen vacancies, metallic defects, and dislocations. According to the filament model, the defects extend to form tiny CFs in the HRS, and these CFs accumulate to form stronger and more localized CFs, leading to the transition from the HRS to LRS. The higher process current and unstable process voltage may result from a large number of defects existing in the HfO_x film. The filaments originating from CFs are formed at random, which may result in different thermal dissipations rupturing different filaments in each reset process. Namely, the filaments may not follow the same path in each switching. Figure 2(c) shows the endurance properties of the device without plasma treatment. Reading was performed at 0.2 V. Although the device could be operated after ~21 program/erase cycles with an on–off ratio of ~10^3, the fluctuation in resistance switching was obviously due to the complicated filament structure in the HfO_x film.

Figure 3(a) shows the typical I–V characteristics of a Ni/HfO_x/Ni memory cell with plasma post-treatment ($CF_4 : O_2 = 10 : 1$) measured at room temperature under dc voltage sweeping, using a forming voltage of ~13 V with a compliance current of 1 μA. After the forming process, the device entered the LRS. By sweeping a positive bias above the reset voltage (V_{reset}) of approximately +0.8 V, an abrupt decrease in current was observed, where the cell switches from the LRS to HRS, called the reset process. Conversely, the cell returned to the LRS upon applying a positive bias above the set voltage (V_{set}) of approximately 2.3 V, called the set process. Figures 3(b) and 3(c) show the I–V curves and the resistance evolution of the two well-resolved states during the initial 55 cycles, respectively. Reading was performed at 0.2 V. The device with plasma post-treatment ($CF_4 : O_2 = 10 : 1$) exhibited more stable resistance at negative voltages and a lower process current at positive voltages than the device without plasma treatment. The improvements may be ascribed to the restoration of some of the defects at the Ni/HfO_x surface and fixed charge defects near the interface formed by fluorine atoms. Owing to the reduction of defects in the HfO_x film, the formation of CFs may be limited to certain local regions, resulting in a small increase in the forming voltage and a decrease in the process current.

Figure 4(a) shows the typical I–V characteristics of a Ni/HfO_x/Ni memory cell with plasma post-treatment ($CF_4 : O_2 = 2 : 8$) measured at room temperature under dc voltage sweeping. The device with plasma treatment ($CF_4 : O_2 = 2 : 8$) exhibited unipolar resistance switching behavior upon applying a forming voltage of ~9.2 V with a compliance current of 100 μA. Resistance switching from the LRS to HRS and *vice versa* were realized at the same polar voltage. After the forming process, the device entered the LRS. By sweeping at a bias above the reset voltage (V_{reset}) of approximately 0.9 V, an abrupt decrease in current was observed, where the cell switches from the LRS to HRS, called the reset process. Conversely, the cell returned to the LRS upon applying a positive bias above the set voltage (V_{set}) of approximately 7 V, called the set process. Figures 4(b) and 4(c) show the I–V curves and the endurance properties of the device with plasma post-treatment ($CF_4 : O_2 = 2 : 8$) during the initial seven cycles, respectively. Reading was performed at 0.2 V. Compared with the cell without plasma

© 2012 The Japan Society of Applied Physics

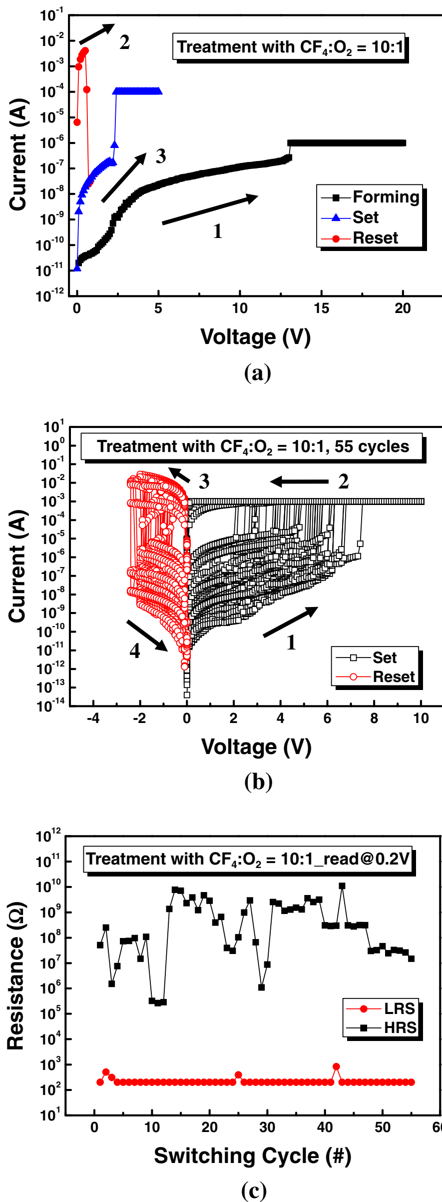

Fig. 3. (Color online) (a) Typical I–V characteristics of RRAM with Ni/HfO_2/Ni capacitor structure, (b) I–V curves for 55 cycles of voltage sweeping, (c) endurance properties for the device with plasma treatment ($CF_4 : O_2 = 10 : 1$).

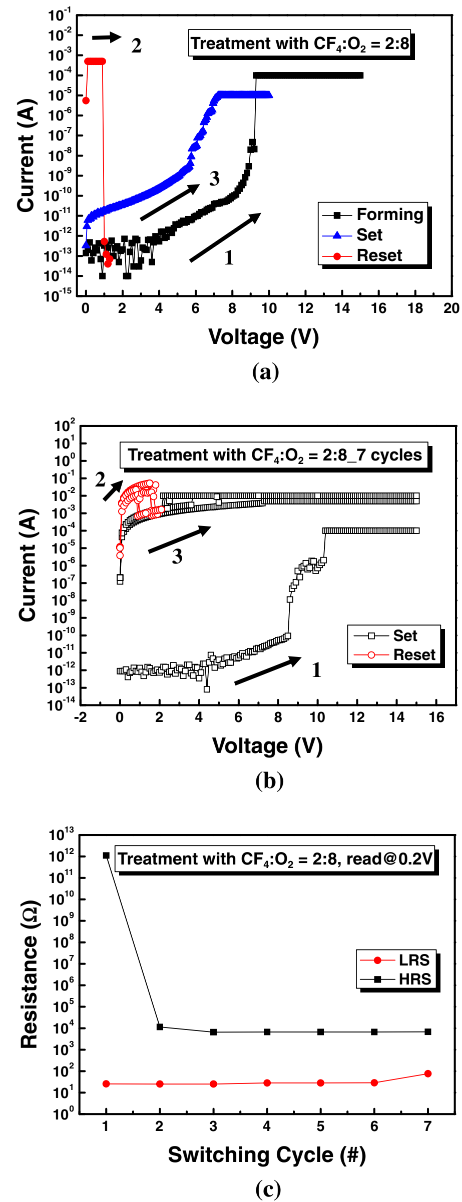

Fig. 4. (Color online) (a) Typical I–V characteristics of RRAM with Ni/HfO_2/Ni capacitor structure, (b) I–V curves for seven cycles of voltage sweeping, (c) endurance properties for the device without plasma treatment ($CF_4 : O_2 = 2 : 8$).

treatment, the device with plasma treatment ($CF_4 : O_2 = 2 : 8$) appeared to be inferior, showing a high leakage current. The HRS current was dominated by ohmic conduction.[21] The positive shift of the reset voltage may be caused by the fixed charge due to the damaged surface layer. In the reset process, the reset voltage became more stable but the endurance decreased. These results may be related to the surface oxide, whose surface quality is improved by plasma post-treatment. The thin oxide layer on the surface provides a higher resistance at a lower operation voltage. With increasing operating voltage, carriers could obtain sufficient energy to produce a tunneling effect. Owing to the use of a higher forming voltage, the surface oxide is very likely to undergo a hard breakdown and resistance degradation, resulting in a reduction of the number of endurance cycles.

Figure 5 shows the crystal structure of the HfO_x film on the Ni/SiO_2/Si substrate investigated by X-ray diffracto-

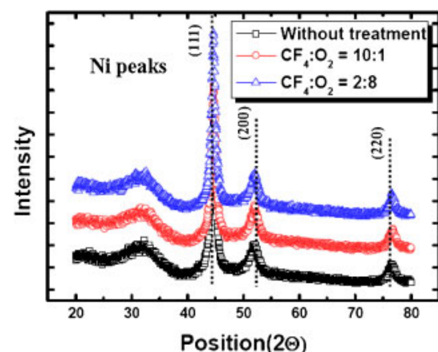

Fig. 5. (Color online) Crystal structure of the HfO_x film on the Ni/SiO_2/Si substrate investigated by X-ray diffractometry.

© 2012 The Japan Society of Applied Physics

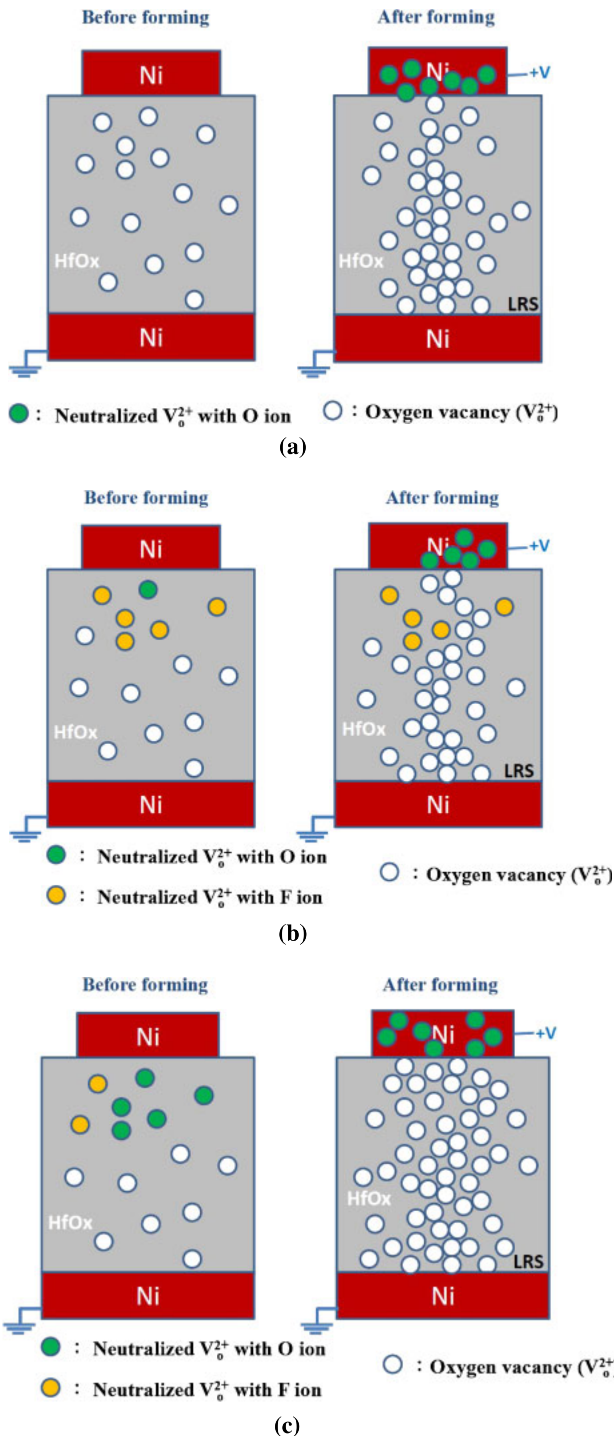

Fig. 6. (Color online) Schematic diagrams of formation of conductive filaments (CFs) for LRS for the device (a) without post-treatment, (b) with plasma post-treatment ($CF_4 : O_2 = 10 : 1$), and (c) with plasma post-treatment ($CF_4 : O_2 = 2 : 8$) after forming process.

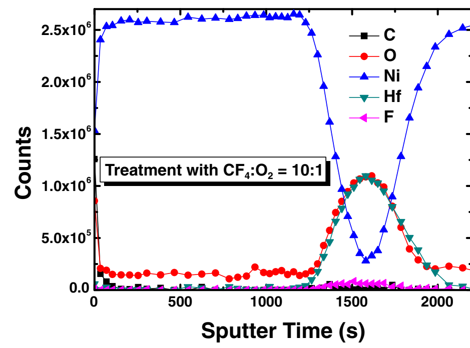

Fig. 7. (Color online) Compositional depth profile of the samples with plasma post-treatment ($CF_4 : O_2 = 10 : 1$).

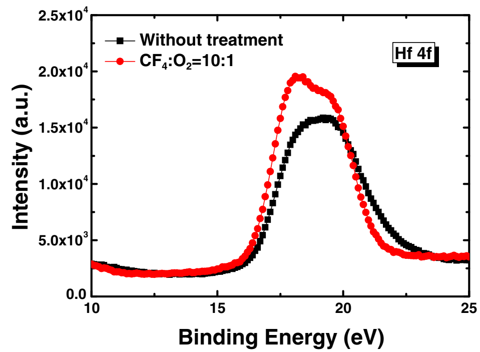

Fig. 8. (Color online) Hf 4f ESCA spectra of the samples with and without plasma post-treatment ($CF_4 : O_2 = 10 : 1$).

metry. No peak was observed around 30–34°. Only the Ni peaks at (111), (200), and (220) were observed, which indicates that the HfO_x film is amorphous. This result may explain the higher initial resistance and the HRS.

Figure 6 shows schematic diagrams of the effects of the incorporation of F atoms on the formation of CFs in the LRS after the forming process. According to the filament model, the formation of CFs in the device without plasma post-treatment was random, and CFs did not follow the same path, causing the fluctuation of resistance switching, as shown in Fig. 6(a). However, the dispersion of resistance switching could be suppressed by suitable CF_4/O_2 plasma post-treatment, and the F atoms confined CF formation to a local region, as shown in Fig. 6(b). During the forming process, the tiny CFs, such as oxygen vacancies, accumulate to form stronger and more localized CFs, which then induce a transition from the HRS to LRS. After the reset process, the disruption of CFs can be caused by oxidation enhanced by Joule heating, and the resulting device can undergo a transition from the LRS to HRS. Because of the F incorporation and the formation of Hf–F bonds by the suitable CF_4/O_2 plasma post-treatment, the existing Hf–F bonds may limit the distribution of some CFs, leading to certain local CFs being disrupted easily. Therefore, the reset voltage and the path of CF formation/rupture can be stabilized by F incorporation, resulting in the stability of resistance switching. Moreover, in the case of plasma post-treatment ($CF_4 : O_2 = 2 : 8$), there were fewer oxygen vacancies in the film. A higher compliance current resulted in the formation of stronger and less resistive filaments, as shown in Fig. 6(c).

The concentration depth profile of the sample with plasma post-treatment ($CF_4 : O_2 = 10 : 1$) measured for various elements is depicted in Fig. 7, showing the stack of layers. Figure 8 shows the Hf 4f ESCA spectra of the samples with and without plasma post-treatment ($CF_4 : O_2 = 10 : 1$). The intensity of the CF_4-treated sample was higher than that of the reference sample and the blurry peak at about 20 eV revealed Hf–F bonding, indicating fluorine incorporation after post-treatment.[22)]

 © 2012 The Japan Society of Applied Physics

4. Conclusions

The resistance switching characteristics of e-gun-evaporator-deposited HfO_2-based ReRAM devices were investigated for the case of CF_4/O_2 plasma treatment with different gas flow rate ratios. It has been demonstrated that oxygen/fluorine incorporation passivated interface traps and/or reduced the fixed charge, which improved the resistance distribution and current in the LRS. The proposed device showed a stable current in the LRS and a stable operating voltage upon suitable plasma treatment owing to the path stability of CFs limited by Hf–F bonds.

Acknowledgements

The authors would like to thank the staff of the National Nano Device Laboratory for their technical help. This work was supported by the National Nano Device Laboratory under Contract No. NDL99-C01S-016 and Chung Hua University under Contract No. CHU-99-E-03.

1) R. Waser: Microelectron. Eng. **86** (2009) 1925.
2) Y.-M. Kim and J.-S. Lee: J. Appl. Phys. **104** (2008) 114115.
3) J.-S. Lee, C.-S. Kang, Y.-C. Shin, C.-H. Lee, K.-T. Park, J.-S. Sel, V. Kim, B.-I. Choe, J.-S. Sim, J. Choi, and K. Kim: Jpn. J. Appl. Phys. **45** (2006) 3213.
4) M. J. Lee, Y. Park, B. S. Kang, S. E. Ahn, C. Lee, K. Kim, W. Xianyu, G. Stefanovich, J. H. Lee, S. J. Chung, Y. H. Kim, C. S. Lee, J. B. Park, I. G. Baek, and I. K. Yoo: IEDM Tech. Dig., 2007, p. 771.
5) K. Aratani, K. Ohba, T. Mizuguchi, S. Yasuda, T. Shiimoto, T. Tsushima, T. Sone, K. Endo, A. Kouchiyama, S. Sasaki, A. Maesaka, N. Yamada, and H. Narisawa: IEDM Tech. Dig., 2007, p. 783.
6) Y. Watanabe, J. G. Bednorz, A. Bietsch, Ch. Gerber, D. Widmer, A. Beck, and S. J. Wind: Appl. Phys. Lett. **78** (2001) 3738.
7) W. Guan, S. Long, Q. Liu, M. Liu, and W. Wang: IEEE Electron Device Lett. **29** (2008) 434.
8) D. S. Jeong, B. J. Choi, and C. S. Hwang: J. Appl. Phys. **100** (2006) 113724.
9) J. Y. Son and Y.-H. Shin: Appl. Phys. Lett. **92** (2008) 222106.
10) K. M. Kim, B. J. Choi, and C. S. Hwang: Appl. Phys. Lett. **90** (2007) 242906.
11) D. C. Kim, S. Seo, S. E. Ahn, D.-S. Suh, M. J. Lee, B.-H. Park, I. K. Yoo, I. G. Baek, H.-J. Kim, E. K. Yim, J. E. Lee, S. O. Park, H. S. Kim, U.-I. Chung, J. T. Moon, and B. I. Ryu: Appl. Phys. Lett. **88** (2006) 202102.
12) S. Lee, W.-G. Kim, S.-W. Rhee, and K. Yong: J. Electrochem. Soc. **155** (2008) H92.
13) I.-S. Park, K.-R. Kim, S. Lee, and J. Ahn: Jpn. J. Appl. Phys. **46** (2007) 2172.
14) H.-Y. Lee, P.-S. Chen, C.-C. Wang, S. Maikap, P.-J. Tzeng, C.-H. Lin, L.-S. Lee, and M.-J. Tsai: Jpn. J. Appl. Phys. **46** (2007) 2175.
15) C. Y. Lin, D. Y. Lee, S. Y. Wang, C. C. Lin, and T. Y. Tseng: Surf. Coatings Technol. **203** (2008) 628.
16) R. Xie, M. Yu, M. Y. Lai, L. Chan, and C. Zhu: Appl. Phys. Lett. **92** (2008) 163505.
17) Y.-T. Chen, H. Zhao, J. H. Yum, Y. Wang, F. Xue, F. Zhou, and J. C. Lee: Appl. Phys. Lett. **95** (2009) 013501.
18) K. Tse and J. Robertson: Appl. Phys. Lett. **89** (2006) 142914.
19) C. S. Lai, W. C. Wu, K. M. Fan, J. C. Wang, and S. J. Lin: Jpn. J. Appl. Phys. **44** (2005) 2307.
20) Y.-T. Chen, H. Zhao, J. H. Yum, Y. Wang, F. Xue, F. Zhou, and J. C. Lee: J. Electrochem. Soc. **157** (2010) G71.
21) K. L. Lin, T. H. Hou, J. Shieh, J. H. Lin, C. T. Chou, and Y. J. Lee: J. Appl. Phys. **109** (2011) 084104.
22) C. S. Lai, W. C. Wu, J. C. Wang, and T. S. Chao: Appl. Phys. Lett. **86** (2005) 222905.

© 2012 The Japan Society of Applied Physics